Journal of Materials Chemistry C

The Effect of Light Environment during Film Formation Process on the Morphology and Function of Organic Photovoltaics

Journal:	*Journal of Materials Chemistry C*
Manuscript ID	TC-ART-06-2019-003443.R1
Article Type:	Paper
Date Submitted by the Author:	25-Jul-2019
Complete List of Authors:	Wu, Xiaomin; Fuzhou University, Institute of Optoelectronic Display, National & Local United Engineering Lab of Flat Panel Display Technology Lan, Shuqiong; Fuzhou University, Institute of Optoelectronic Display, National & Local United Engineering Lab of Flat Panel Display Technology Zhang, Guocheng; Fuzhou University, Institute of Optoelectronic Display, National & Local United Engineering Lab of Flat Panel Display Technology Chen, Huipeng; Fuzhou University, Institute of Optoelectronic Display, National & Local United Engineering Lab of Flat Panel Display Technology Guo, Tailiang; Fuzhou University, National & Local United Engineering Laboratory of Flat Panel Display Technology

The Effect of Light Environment during Film Formation Process on the Morphology and Function of Organic Photovoltaics

Xiaomin Wu[a], Shuqiong Lan[a], Guocheng Zhang[b], Huipeng Chen[a,*] and Tailiang Guo[a]

[a] Institute of Optoelectronic Display, National & Local United Engineering Lab of Flat Panel Display Technology, Fuzhou University, Fuzhou 350002, China. Email: hpchen@fzu.edu.cn
[b] College of Information Science and Engineering, Fujian University of Technology, Fuzhou 350108, China

Abstract

In reported fabrication process of organic photovoltaics (OPV), light environment is usually thought to be negligible and missing in the experimental section. In this work, the morphology of organic bulk-heterojunction (BHJ) photovoltaics in the presence and absence of white light during film formation process is examined by small angle neutron scattering and grazing incidence x-ray scattering. It provids the first clear experimental evidence that the morphology, thermodynamics and function of BHJ blends is significantly impacted by the photo absorption during film formation process. The results clearly demonstrate that crystal sizes of donor material decrease and the size of pure acceptor phase increases with an increase of light intensity along with enhanced acceptor aggregates. Moreover, the specific interfacial area between pure acceptor phase and its surrounding matrix is found to be crucial for the electron transport and device performance, which reaches maximum with the presence of 1 sun, resulting in the best device performance. The generalization of the impact of light illumination is also investigated in other OPV systems including fullerene and non-fullerene systems.

This finding can open the door to a wide range of applications of simple illumination on the processing of organic semiconductor based devices to precise control the morphology and surely expend the application of illumination for further improvement of OPV performance.

1. Introduction

With the increasing interest in organic semiconductors for using in organic photovoltaics, organic light emitting diodes, and field effect transistors, the understanding of the chain conformation of organic semiconductors becomes extremely important, as its optoelectronic properties are highly dependent on the chain conformation of the organic semiconductors.[1-9] The interaction of organic semiconductors with light leads to photo excitations, forming excitons, which can travel along and across the semiconducting chains. The resulting excitation from light absorption is transferred via a variety of intra- or intermolecular transfer mechanisms, resulting in desirable optoelectronic properties, i.e. photoluminescence. One might envision that the movement of charges along the semiconducting chain can constrict or expand the semiconducting chain, altering its conformation with exposure to light. Reiter and coworkers found that the dewetting of a mixture of polystyrene and conjugated polymer was faster in the dark than when it was exposed to light.[10] They interpreted this result to indicate that the exposure to light increased film viscosity and expanded the conjugated chains, slowing their motion. A similar polymer blend was examined in a related work, which showed that the photoluminescent intensity increased up to 40% with exposure to white light.[11] It is attributed to the formation of

exciton under light exposure, which would force the planarization of MEH-PPV chains. Moreover, Morgan and Dadmun investigated chain conformation of conjugated polymer in solution under illumination and the results indicated that the Kuhn length and radius of gyration significantly decreased upon light exposure.[12] They proposed that the interaction of light with the backbone of conjugated polymers altered their solubility in and thermodynamic interaction with their surrounding solvents. Furthermore, recently Amita and coworkers reported that illumination had strong impact on the rate of metal halide perovskite formation and subsequent film morphology.[13] They claimed that the generation of electron-hole pairs would lead to the light-activated nucleation. The number of charge carriers trapped at the PbI_2 surface would increase with an increase of light intensity, resulting in a decrease of surface tension and an increase nucleation density.

Meanwhile, organic photovoltaics (OPV) based on the bulkhetrojuction (BHJ) blends of organic donor and acceptor, have attracted much attention over the past decades because of their advantages, such as light weight, low cost, and flexible. The morphology of BHJ blends has been considered to be crucial for OPV device performance.[14-25] Therefore, there is now a large body of literature on various ways to control the morphology of BHJ blends including thermal annealing, solvent annealing, co-solvents, and solvent additives.[26-37] Meanwhile, the reports above clearly demonstrated that illumination would affect the chain conformation of organic semiconductors in solution, film formation kinetics and subsequent morphology. Therefore, there is little doubt that illumination would provide an alternative strategy

to optimize the morphology of organic photovoltaics via altering the chain confirmation and thermodynamic interaction during film formation process. Unfortunately, the effect of illumination during film formation process on the morphology of organic photovoltaics has never been reported. More importantly, fundamental understanding of how photon absorption by a semiconductor alters its morphology, dynamics and thermodynamics in blends would provide previously unavailable information about the potential application of light exposure in OPV. Moreover, correlation of local structural changes to the macroscopic dynamic response of the blends in the presence and absence of illumination will probe the fundamental processes which hierarchically guide the change in macroscopic behavior of BHJ blends as a result of photon absorption.

Hence, in this work the effect of illumination during film formation process on the morphology of organic BHJ solar cells including fullerene and non-fullerene systems was examined owing to several attractive properties of non-fullerene systems.[38-40] It indicated that the morphology and thermodynamics of organic BHJ blends was significantly impacted by photo absorption, which in turn impacts OPV device performance. The results revealed that the crystal size of organic donor decreased with an increase of light intensity. Moreover, small angle neutron scattering (SANS) results demonstrated that the acceptor phase separation was significantly impacted by photo absorption. The optimized morphology was achieved with illumination with proper intensity, resulting in best device performance. This finding would provide a more precise morphologic control of organic photovoltaics with photo absorption and surely

expend the application of illumination for further improvement of OPV device performance.

2. Experimental section

p-DTS(FBTTh$_2$)$_2$ and PC$_{70}$BM were purchased from 1-Materials. Solution of active layer was prepared by dissolving p-DTS(FBTTh$_2$)$_2$ (15 mg/mL) and PC$_{70}$BM (10 mg/mL) in chlorobenzene with 0.4 vol% diiodooctane. The active layers were fabricated by blade coating at a constant speed of 5 mm/s. The substrate temperature was kept at 60 °C and the gap between the knife blade and substrate was 100 μm. The films were then baked at 100 °C for 10 mins in glove box to remove residual solvents. The blade coating was performed in the presence and absence of illumination, using a power-tunable white LED purchased from Zhenzheng Optoelectronics Company. The irradiation spectrum of the white LED obtained from Spectral luminance meter (SRC-200M) was provided in **Fig. S1.** Four light intensities including 0 Sun, 0.5 Sun, 1 Sun, and 2 Sun were selected in this work, where 0 Sun refers to the dark and 1 Sun refers to a light intensity of 100 mW cm^{-2}. The resultant film thickness was about 98 nm for all the films.

Atomic force microscopy (AFM) (Bruker NanoScope V) was employed to characterize the surface morphology of active layers The thickness of the active layers was measured by a depth profiler (BRUKER, DektakXT). X-ray photoelectron spectroscopy (XPS) experiments were carried out in an ESCALAB 250 X-ray photoelectron spectroscopy. Grazing incidence wide-angle x-ray scattering (GIWAXS) experiments were done at beamline BL14B1, Shanghai Synchrotron Radiation Facility.

The intensity and wavelength of x-ray beam was 10 Kev and 0.1236 nm, respectively. Small-angle neutron scattering experiments (SANS) were conducted at the Oak Ridge National Laboratory for Neutron Research (beamline CG2). The raw data were corrected with empty cell scattering, detector sensitivity, and dark current, which were then calibrated to an absolute intensity using a Porasil-A standard. The scattering length density (SLD) of p-DTS(FBTTh$_2$)$_2$ and PC$_{70}$BM is 1.2 × 10^{-4} nm^{-2} and 4.5 × 10^{-4} nm^{-2}, respectively.[41] Surface energy of neat p-DTS(FBTTh$_2$)$_2$ and PC$_{70}$BM was determined from contact-angle measurements (Kino SL200KS) , which was evaluated by geometric mean using the contact angle of diiodomethane and water on the surface of the solid films. The surface energy of p-DTS(FBTTh$_2$)$_2$ and PC$_{70}$BM are 28.4 and 37.8 mJ/m^2, respectively.

The devices were fabricated with a conventional structure of ITO/PEDOT:PSS/ p-DTS(FBTTh$_2$)$_2$:PCBM/Ca/Al. A thin layer of PEDOT:PSS was spin-coated with 4000 rpm for 20 seconds onto the cleaned ITO substrate and then immediately annealed in air at 140 °C for 20 minutes. Then, p-DTS(FBTTh$_2$)$_2$:PC$_{70}$BM blends were blade coated on PEDOT:PSS as described above. Finally, a thin layer of Ca (5 nm) and then 100 nm Al layer were evaporated under high vacuum. The Current density-voltage (J-V) characteristics of the devices were measured under AM 1.5G (100 mW/cm^2) using Sun 2000, Abet Technologies. The light intensity was calibrated with a single-crystal Si-based solar cell. The hole and electron mobility of the blend films were measured using the SCLC (space-charge limited current) method by fitting of the dark current, with device structures of ITO/PEDOT:PSS/ p-DTS(FBTTh$_2$)$_2$:PCBM /MoO$_3$/Al (hole-only

device) and ITO/ZnO/PFN/p-DTS(FBTTh$_2$)$_2$:PCBM/PFN/Al (electron-only device).

3. Results

Fig. 1 showed the tapping-mode AFM images of p-DTS(FBTTh$_2$)$_2$:PCBM thin films under different illumination conditions. The results clearly showed that p-DTS(FBTTh$_2$)$_2$:PCBM films exhibited well inter-connected network structure and the crystal sizes became smaller with an increase of light intensity. **Fig. 2** presented the out-of-plane and in-plane profiles extracted from 2D grazing incidence x-ray scattering (GIWAXS) patterns of p-DTS(FBTTh$_2$)$_2$:PCBM thin films. The (100) diffraction peak located at q ≈3.2 nm^{-1} in out-of-plane curves was observed for all the blends, which is correlated to lamellar spacing of p-DTS(FBTTh$_2$)$_2$ separated by the side chains.[42] The (100) peak position almost remained unchanged with the change of illumination conditions, which indicated that the lamellar distance of p-DTS(FBTTh$_2$)$_2$ was not impacted by photo absorption. Moreover, the lamellar coherence length, which is associated with the crystalline domain size was determined by the Scherrer's equation and listed in **Table 1**.[43, 44] The results showed that the coherence length decease with an increase of light intensity, indicating a decrease of p-DTS(FBTTh$_2$)$_2$ crystal sizes, which was consistent with AFM results. Furthermore, the peak area of (100) peak was almost unchanged with photo absorption, which indicated that the p-DTS(FBTTh$_2$)$_2$ crystallinity remained constant for all the samples. Meanwhile, the (010) peak at q =17.3 nm^{-1} was observed in all the samples in the in-plane direction, which was relevant to π-π stacking of p-DTS(FBTTh$_2$)$_2$ molecules. The peak position almost maintained invariant for all the samples, which clearly illustrated that the π-π stacking distance

within the crystal that was crucial for charge transport, was independent to photo absorption.

The GIWAXS results only provided information about the molecular packing and crystallization of donor materials. Thus, small angle neutron scattering (SANS) was employed to provide information on the alteration of the fullerene phase separation under different illumination conditions. The SANS curves were presented in **Fig. 3**. In SANS, the scattering intensity is proportional to the square of the difference of the SLD of two phases. Therefore, the increase of scattering intensity indicated an enhancement of PCBM phase separation with light illumination. Similar to P3HT (SLD=0.7 × 10^{-4} nm^{-2}):PCBM system, as SLD of the PCBM (4.5 × 10^{-4} nm^{-2}) is significant larger than p-DTS($FBTTh_2$)$_2$ (1.2 × 10^{-4} nm^{-2}), the SANS scattering is dominated by pure PCBM phase. Thus, the domain sizes and specific interfacial areas obtained from SANS referred to the pure PCBM phase dispersed in its surrounding matrix.[45, 46]

In order to obtain more detailed structure information, the scattering curves were fitted to Schulz sphere model, which has been successfully used to describe the dispersion of pure fullerene phase within its surrounding matrix in the organic donor:fullerene systems.[47, 48] As shown in Fig. 3a, the SANS curves were well fitted to Schulz sphere model, from which polydispersity of the pure PCBM domains (P), volume fraction of pure PCBM phase (Φag), size of pure PCBM agglomeration (Ra), and specific interfacial area (S/V) between pure PCBM phase and its surrounding matrix in the whole samples can be obtained and listed in Table 1. The results showed that volume fraction of pure PCBM phase increased obviously from 13.2% up to 23.3%

with an increase of light intensity. Fig. 3b showed the distribution of pure PCBM domains obtained from Schulz sphere model. The sample under dark provided an average radius of 71 Å with polydispersity of 0.27. with an increase of light intensity, polydispersity of the pure PCBM domains increased from 0.27 to 0.40, size of pure PCBM agglomeration increased from 71 Å to 100 Å, and S/V increased firstly and then decreased with the maximum of 573945 cm^{-1} under 1sun.

To examine the vertical phase separation of p-DTS($FBTTh_2$)$_2$:PCBM blends, the surface composition of was p-DTS($FBTTh_2$)$_2$ evaluated by XPS. In XPS, the atomic ratio of N(2p)/C(1s) and S(2p)/C(1s) was proportional to the surface composition of p-DTS($FBTTh_2$)$_2$. As shown in **Table 2**, the atomic ratio of N(2p)/C(1s) and S(2p)/C(1s) increased with an increase of light intensity , which indicated an increase of p-DTS($FBTTh_2$)$_2$ concentration and decrease of PCBM concentration at active layer/air interface. The vertical phase separation in BHJ blends is believed to be related to the difference in the surface energy of each component. Similar to P3HT:PCBM, as p-DTS($FBTTh_2$)$_2$ has a lower surface energy than PCBM, p-DTS($FBTTh_2$)$_2$ tended to accumulate at the air surface in order to reduce the overall energy. Therefore, the enhancement of p-DTS($FBTTh_2$)$_2$ aggregation at the air surface indicated that the vertical phase separation of p-DTS($FBTTh_2$)$_2$ was enhanced with an increase of light intensity. Moreover, the enhancement of p-DTS($FBTTh_2$)$_2$ aggregation indicated an depletion of PCBM at the air surface (near the cathode) with photo absorption, which would inhibit efficient charge transport and charge collection near the cathode, and thus deteriorate the device performance. The nanomorphology of the system was

schematically presented in **Fig. 4**, which showed the enhancement of PCBM phase separation and the depletion of PCBM at the air surface.

The results above clearly revealed that the morphology of active layer was significantly impacted by the photo absorption during film formation process. To make this information more valuable, these morphologic changes must be correlated to photovoltaic properties. For this purpose, the device performance of all the samples was measured, and the results were presented in **Fig. 5** and Table 2. The device performance of blend obtained under indoor light environment (0.2 Sun) was provided in **Fig. S2**. The device under dark condition exhibited a PCE of 6.8% with a short-circuit current density (Jsc) of 12.7 mA cm^{-2}, Voc of 0.84 V and FF of 63.8%. The device performance was first enhanced with an increase of light intensity and the best device was found in the device, whose active layer was developed under 1 Sun, where the PCE increased to 9.0%. However, further increase of light intensity lead to a decrease of PCE to 8.0%. Furthermore, the electron and hole mobility obtained from space charge limited current (SCLC) measurements were presented in Fig. 5 and **Table 3**. The results showed that the hole mobility increased with an increase of light intensity, while the maximum electron mobility was achieved in the device fabricated under 1 Sun.

4. Discussion

To the best of our knowledge, this work provides the first clear experimental evidence that the morphology and thermodynamics of organic BHJ blends was significantly impacted by photo absorption during film formation process, which in turn impacted OPV device performance.

The interaction of organic semiconductors with light leads to photo excitations, and formation of excitons, electron-hole pairs. Excess photo-generated carriers were populated at the surface of organic semiconductor.[13] According to Lippmanm's equation, the surface tension can be expressed as

$$\gamma = \gamma_0 - \frac{\sigma^2}{2C_0}$$

where γ_0 is the surface tension at zero charge, σ is the excess surface charge and C_0 is the double-layer capacitance.[49, 50] Therefore, an increase of excess surface charge would lower the value of surface tension as a result of photo absorption. This is consistent with XPS results, which showed an increase of p-DTS(FBTTh$_2$)$_2$ concentration at the air surface, indicating a decrease of surface energy. Moreover, the decease of surface tension lowers the critical free energy of nucleation and the critical nucleus size, resulting in formation of smaller crystals.[51, 52] This is consistent with AFM and GIWAXS results, showing an decease of p-DTS(FBTTh$_2$)$_2$ crystal sizes.

Moreover, the SANS results revealed that PCBM phase separation was enhanced with illumination. It is associated with the decrease of surface tension of p-DTS(FBTTh$_2$)$_2$ as a result of photo absorption. As surface energy of p-DTS(FBTTh$_2$)$_2$ (28.4 mJ/cm^2) is lower than PCBM (37.8 mJ/cm^2), the decrease of surface energy of p-DTS(FBTTh$_2$)$_2$ would increase the difference of surface energy between p-DTS(FBTTh$_2$)$_2$ and PCBM, leading to less compatible blends and enhancement of PCBM phase separation.

Similar to P3HT:PCBM blends, the BHJ blends consist of three phases in the p-DTS(FBTTh$_2$)$_2$:PCBM mixture: a p-DTS(FBTTh$_2$)$_2$ crystalline phase, a pure PCBM

phase, and a mixing phase of non-crystalline p-DTS($FBTTh_2$)$_2$ and PCBM. The existence of the mixing phase would benefit efficient exciton dissociation as there is ample donor/acceptor interfacial area in this phase, which also indicated that most charge carriers are generated in this area. Meanwhile, due to the coexistence of electron and holes in this area, a higher probability of bimolecular recombination is predicted. To reach the electrode, the electrons that are generated in the mixing phase should transport in the mixing phase to the electrode or transport through pure PCBM phase to the electrode. Therefore, the presence of pure PCBM phase, especially a larger interfacial area (S/V) between pure PCBM phase and its surrounding matrix would provide additional pathways connecting pure PCBM phase and the mixing phase, which facilitates the electrons to escape from the "slow pathway" miscible phase to the "fast pathway" pure PCBM phase, resulting in the reduction of bimolecular recombination and enhancement of PCE. This is verify by electron mobility measurements and device performance tests, which showed that the highest electron mobility and best device performance was obtained in the device fabricated under 1 Sun, which exhibited highest S/V value. The storage stability of p-DTS($FBTTH_2$)$_2$:PCBM device were tested and the results were shown in **Figure S3.** It showed similar normalized PCE as function of AM 1.5G illumination time, indicating that light processing during device fabrication mainly affected the morphology of active layer and has less impact on the storage stability. **Figure S4** presented the normalized UV–vis spectra of p-DTS($FBTTH_2$)$_2$:PCBM devices obtained from different light intensities. It showed that almost the same UV-vis spectrum was found for each sample, which indicated that

photo-degradation and/or photo-oxidation of organic materials did not occur during 1sun/2sun illumination process.

To investigate whether the impact of light illumination could be generalized to other organic photovoltaic systems including fullerene systems and non-fullerene systems, the photovoltaic properties of P3HT:PCBM, PTB7-th:PCBM, PCDTBT:PCBM, PCDTBT:PCBM, and PBDB-T:ITIC[53] bends obtained from different light illumination were measured. The J-V curves were presented in **Fig. S5** and the results were tabulated in Table S1 and been contrasted in **Fig. 6**. It showed that the PCE of the devices were significantly affected by the light illumination, which supported our findings. For the fullerene systems, as fullerene usually has higher surface energy than organic donor, the decrease of surface energy of organic donor with light illumination during film formation would enhance the surface energy difference between donor and acceptor, resulting in the enhancement of phase separation. It should be noted that light illumination during film formation impacts the surface energy of organic semiconductors, which in turns to affect the phase separation of BHJ blends, but it would not guarantee the improvement of device performance. For instance, in the PCDTBT:PCBM (1:2) blends, light illumination enhanced the phase separation of BHJ blends, leading to the increase of PCE. However, for PCDTBT:PCBM (1:4) blends, excess phase separation with light illumination would deteriorate the device performance. For the PBDB-T:ITIC devices, the change of surface energy of PBDB-T and ITIC during film formation with light illumination, resulting in enhanced phase separation, as shown in **Fig. S6.**

Hence, this finding offered hierarchical guides for the change in macroscopic behavior of BHJ blends as a result of photon absorption. It can be used to optimize the morphology of donor:acceptor blends with various miscibility. Ade and coauthors reported the miscibility-function relationship where percolation threshold is the ideal morphology for donor:acceptor blends while too pure (low miscibility) or too miscible would lead to bad device performance.[54] Fortunately, light illumination would be a powerful tool to tune the morphology towards to the ideal percolation threshold. For instance, for the fullerene system, light illumination was suggested for the film fabrication process for the too miscible blends to ensure there is sufficient pure acceptor phase for percolation threshold; while dark environment was preferred for the film evolution process of BHJ blends with low miscibility to ensure there is ample donor/acceptor interface for efficient exciton dissociation to reach percolation threshold. Meanwhile, this work also indicated that it should be very careful about the light environment during the fabrication of OPV, which impacts its morphology and function. Moreover, this method would also be applicable to multi-component organic semiconductor systems to guide the morphology control.

5. Conclusion

This work provides the first clear experimental evidence that the morphology, thermodynamics and device performance of BHJ blends was significantly impacted by the light environment during film formation process. Careful data analysis indicated that donor crystal sizes decreased and the size of pure acceptor phase increased with an increase of light intensity along with enhanced acceptor phase separation. It is

associated with the decrease of surface energy of donor material as a result of photo absorption, which enhanced the surface energy difference between donor and acceptor, leading to enhanced acceptor phase separation.

More importantly, this work is a unique example to demonstrate that crystallization of donor and acceptor phase separation can be efficiently tuned by photo absorption during film formation process. Meanwhile, significant impact of light illumination on the photovoltaic properties was also observed in other OPV systems including fullerene and non-fullerene systems. This finding would provide a more precise morphologic control of organic photovoltaics with photo absorption and surely expend the application of illumination for further improvement of OPV device performance. Moreover, the finding of this effect would open the door to a wide range of applications of simple illumination on the processing of organic semiconductor based devices to tune their local structure and macroscopic properties. Furthermore, this work also indicated that it should be very careful about the light environment during the fabrication of OPV or other multi-component organic semiconductor systems, which impacts its morphology and function.

Conflicts of interest

There are no conflicts to declare.

Acknowledgements

The authors are grateful for financial support from National Natural Science Foundation of China (51503039) and National Key Research and Development Program of China (2016YFB0401103). Part of this work at ORNL's HFIR was sponsored by the

Scientific User Facilities Division, Office of Basic Energy Sciences, US Department of Energy. The authors thank Shanghai Synchrotron Radiation Facility (BL14B1) for providing beamtime and help for GIWAXS experiments.

Notes and references

1 B. J. Schwartz, *Annu. Rev. Phys. Chem.*, 2003, **54**, 141-172.

2 R. Chang, J. Hsu, W. Fann, K. Liang, C. Chang, M. Hayashi, J. Yu, S. Lin, E. Chang and K. Chuang, *Chem. Phys. Lett.*, 2000, **317**, 142-152.

3 S. Heun, R. Mahrt, A. Greiner, U. Lemmer, H. Bassler, D. Halliday, D. Bradley, P. Burn and A. Holmes, *J. Phys.: Condens. Matter*, 1993, **5**, 247-252.

4 J. Yu, D. Hu and P. F. Barbara, *Science*, 2000, **289**, 1327-1330.

5 G. Boschetto, M. Krompiec and C.-K. Skylaris, *J. Phys. Chem. C*, 2018, **122**, 17024-17034.

6 F. Wang, K. Hashimoto, H. Segawa and K. Tajima, *ACS Appl. Mater. Inter.,* 2018, **10**, 8901-8908.

7 L. Huo, X. Xue, L. Tao, W. Xiong and Y. Sun, *Chem. Mater.,* 2018, **30**, 3294-3300.

8 S. Jain, *Sci. Technol. Adv. Mater.*, 2018, **19**, 194-202.

9 Z. Zhang, J. Yu, X. Yin, Z. Hu and W. Tang, *Adv. Funct. Mater.*, 2018, **28**, 1705095-1705102.

10 I. Botiz, P. Freyberg, N. Stingelin, A. C.-M. Yang and G. Reiter, *Macromolecules*, 2013, **46**, 2352-2356.

11 I. Botiz, P. Freyberg, C. Leordean, A. M. Gabudean, S. Astilean, A. C. Yang and N. Stingelin, *ACS Appl. Mater. Interfaces*, 2014, **6**, 4974-4979.

12 B. Morgan and M. D. Dadmun, *Macromolecules*, 2016, **49**, 3490-3496.

13 A. Ummadisingu, L. Steier, J. Y. Seo, T. Matsui, A. Abate, W. Tress and M. Gratzel, *Nature*, 2017, **545**, 208-212.

14 G. Zhang, K. Zhang, Q. Yin, X. F. Jiang, Z. Wang, J. Xin, W. Ma, H. Yan, F. Huang and Y. Cao, *J. Am. Chem. Soc.*, 2017, **139**, 2387-2395.

15 B. Qiu, L. Xue, Y. Yang, H. Bin, Y. Zhang, C. Zhang, M. Xiao, K. Park, W. Morrison, Z.-G. Zhang and Y. Li, *Chem. Mater.*, 2017, **29**, 7543-7553.

16 X. Wu, S. Lan, G. Zhang, Q. Chen, H. Chen and T. Guo, *Adv. Funct. Mater.*, 2017, **27**, 1703268-1703277.

17 H. Zhang, H. Yao, J. Hou, J. Zhu, J. Zhang, W. Li, R. Yu, B. Gao, S. Zhang and J. Hou, *Adv. Mater.*, 2018, **30**, 1800613-1800619.

18 J. Min, X. Jiao, V. Sgobba, B. Kan, T. Heumüller, S. Rechberger, E. Spiecker, D. M. Guldi, X. Wan, Y. Chen, H. Ade and C. J. Brabec, *Nano Energy*, 2016, **28**, 241-249.

19 L. Zhang, B. Lin, B. Hu, X. Xu and W. Ma, *Adv. Mater.*, 2018, **30**, 1800343-1800350.

20 B. Sheng, Z. Ouyang, Q. Guo and C. Jiang, *Rsc Advances*, 2018, **8**, 6519-6526.

21 C. Mcdowell, M. Abdelsamie, M. F. Toney and G. C. Bazan, *Adv. Mater.*, 2018, **30**, 1707114-1707143.

22 S. Xin, N. Gasparini, Y. Long, H. Yao, J. Hou, H. Ade and D. Baran, *ACS Energy Lett.*, 2018, **3**, 669-676.

23 H. L. Hsu, Y. C. Chao, Y. H. Liao, C. L. Chung, Y. J. Peng, C. P. Chen and R. J. Jeng, *ACS Appl. Mater. Interfaces*, 2018, **10**, 8885-8892.

24 L. Ye, Y. Xiong, S. Li, M. Ghasemi, N. Balar, J. Turner, A. Gadisa, J. Hou, B. T. O'Connor and H. Ade, *Adv. Funct. Mater.*, 2017, **27**, 1702016-1702025.

25 L. Ye, H. Hu, M. Ghasemi, T. Wang, B. A. Collins, J. H. Kim, K. Jiang, J. H. Carpenter, H. Li, Z. Li, T. McAfee, J. Zhao, X. Chen, J. L. Y. Lai, T. Ma, J. L. Bredas, H. Yan and H. Ade, *Nat. Mater.*, 2018, **17**, 253-260.

26 H. Chen, S. Hu, H. Zang, B. Hu and M. Dadmun, *Adv. Funct. Mater.*, 2013, **23**, 1701-1710.

27 K. R. Graham, P. M. Wieruszewski, R. Stalder, M. J. Hartel, J. Mei, F. So and J. R. Reynolds, *Adv. Funct. Mater.*, 2012, **22**, 4801-4813.

28 F. Liu, Y. Gu, C. Wang, W. Zhao, D. Chen, A. L. Briseno and T. P. Russell, *Adv. Mater.*, 2012, **24**, 3947-3951.

29 C. R. McNeill, J. J. M. Halls, R. Wilson, G. L. Whiting, S. Berkebile, M. G. Ramsey, R. H. Friend and N. C. Greenham, *Adv. Funct. Mater.*, 2008, **18**, 2309-2321.

30 Q. Wan, X. Guo, Z. Wang, W. Li, B. Guo, W. Ma, M. Zhang and Y. Li, *Adv. Funct. Mater.*, 2016, **26**, 6635-6640.

31 M. M. Wienk, M. Turbiez, J. Gilot and R. A. J. Janssen, *Adv. Mater.*, 2008, **20**, 2556-2560.

32 F. C. Wu, Y. H. Li, C. J. Tsou, K. C. Tung, C. T. Yen, F. S. Chou, F. C. Tang, W. Y. Chou, J. Ruan and H. L. Cheng, *ACS Appl. Mater. Inter.*, 2015, **7**, 18967-18976.

33 Y. Xie, W. Zhou, J. Yin, X. Hu, L. Zhang, X. Meng, Q. Ai and Y. Chen, *J. Mater.Chem. A*, 2016, **4**, 6158-6166.

34 M. Zhang, X. Guo and Y. Li, *Adv. Energy Mater.*, 2011, **1**, 557-560.

35 T. A. Bull, L. S. Pingree, S. A. Jenekhe, D. S. Ginger and C. K. Luscombe, *ACS nano*, 2009, **3**, 627-636.

36 P. Cheng, C. Yan, Y. Li, W. Ma and X. Zhan, *Energ. Environ. Sci.*, 2015, **8**, 2357-2364.

37 P. Cheng, L. Ye, X. Zhao, J. Hou, Y. Li and X. Zhan, *Energ. Environ. Sci.*, 2014, **7**, 1351-1356.

38 P. Cheng, G. Li, X. Zhan and Y. Yang, *Nat. Photonics*, 2018, **12**, 131-142.

39 C. Yan, S. Barlow, Z. Wang, H. Yan, A. K. Y. Jen, S. R. Marder and X. Zhan, *Nat. Rev. Mater.*, 2018, **3**, 18003-18021.

40 Y. Lin, F. Zhao, Y. Wu, K. Chen, Y. Xia, G. Li, S. K. Prasad, J. Zhu, L. Huo, H. Bin, Z. G. Zhang, X. Guo, M. Zhang, Y. Sun, F. Gao, Z. Wei, W. Ma, C. Wang, J. Hodgkiss, Z. Bo, O. Inganas, Y. Li and X. Zhan, *Adv. Mater.*, 2017, **29**, 1604155-1604163.

41 S. Lan, H. Yang, G. Zhang, X. Wu, W. Ning, S. Wang, H. Chen and T. Guo, *The J. Phys. Chem. C*, 2016, **120**, 21317-21324.

42 J. A. Love, C. M. Proctor, J. Liu, C. J. Takacs, A. Sharenko, T. S. van der Poll, A. J. Heeger, G. C. Bazan and T.-Q. Nguyen, *Adv. Funct. Mater.*, 2013, **23**, 5019-5026.

43 S. Lilliu, T. Agostinelli, E. Pires, M. Hampton, J. Nelson and J. E. Macdonald, *Macromolecules*, 2011, **44**, 2725-2734.

44 M. Shao, J. Keum, J. Chen, Y. He, W. Chen, J. F. Browning, J. Jakowski, B. G. Sumpter, I. N. Ivanov, Y. Z. Ma, C. M. Rouleau, S. C. Smith, D. B. Geohegan, K. Hong and K. Xiao, *Nat. Commun.*, 2014, **5**, 3180-3190.

45 S. Lan, H. Yang, G. Zhang, X. Wu, Q. Chen, L. Chen, H. Chen and T. Guo, *ACS Appl. Mater. Interfaces*, 2017, **9**, 20679-20685.

46 H. Chen, Y.-C. Hsiao, B. Hu and M. Dadmun, *Adv. Funct. Mater.*, 2014, **24**, 5129-5136.

47 J. W. Kiel, B. J. Kirby, C. F. Majkrzak, B. B. Maranville and M. E. Mackay, *Soft Matter*, 2010, **6**, 641-646.

48 H. Chen, J. Peet, Y.-C. Hsiao, B. Hu and M. Dadmun, *Chem. Mater.*, 2014, **26**, 3993-4003.

49 D. Kramer, *Phys. Chem. Chem. Phys.*, 2008, **10**, 168-177.

50 A. J. Bard, L.R. Faulkner, A. Bard, L. Faulkner, *Electrochemical methods: fundamentals and applications*, Wiley, Hoboken, NJ, USA 2001.

51 L. Ratke, P.W. Voorhees, G*rowth and coarsening: Ostwald ripening in material processing*, Springer Berlin, Heidelberg, Germany 2002.

52 R. W. Balluffi, S. M. Allen, W. C. Carter, *Kinetics of Materials*, Wiley, Hoboken, NJ, USA 2005.

53 Y. Lin, J. Wang, Z. G. Zhang, H. Bai, Y. Li, D. Zhu and X. Zhan, *Adv. Mater.*, 2015, **27**, 1170-1174.

54 L. Ye, B. A. Collins, X. Jiao, J. Zhao, H. Yan and H. Ade, *Adv. Energy Mater.*, 2018, **8**, 1703058-1703072.

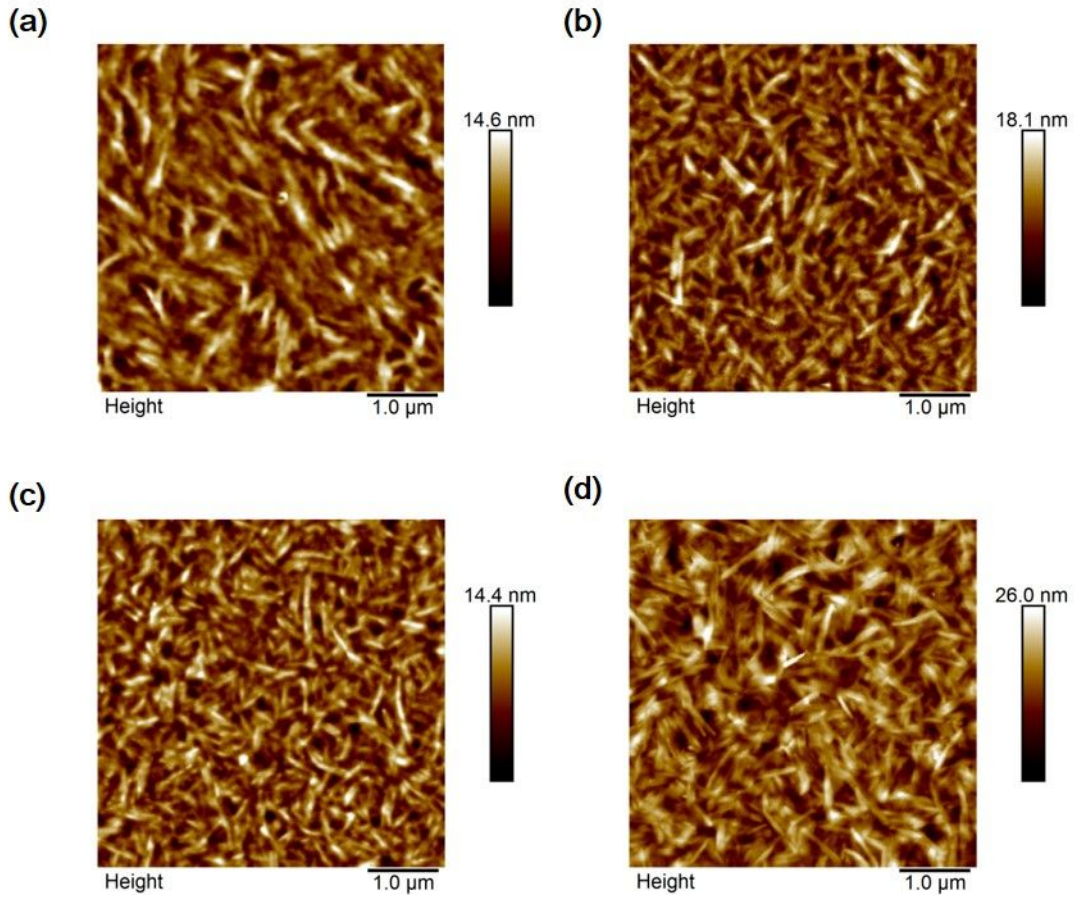

Fig. 1 AFM tapping mode topographies of the surfaces of p-DTS($FBTTH_2$)$_2$:PCBM blends obtained from light intensity of (a) Dark (b) 0.5 Sun (c) 1 Sun (d) 2 Sun.

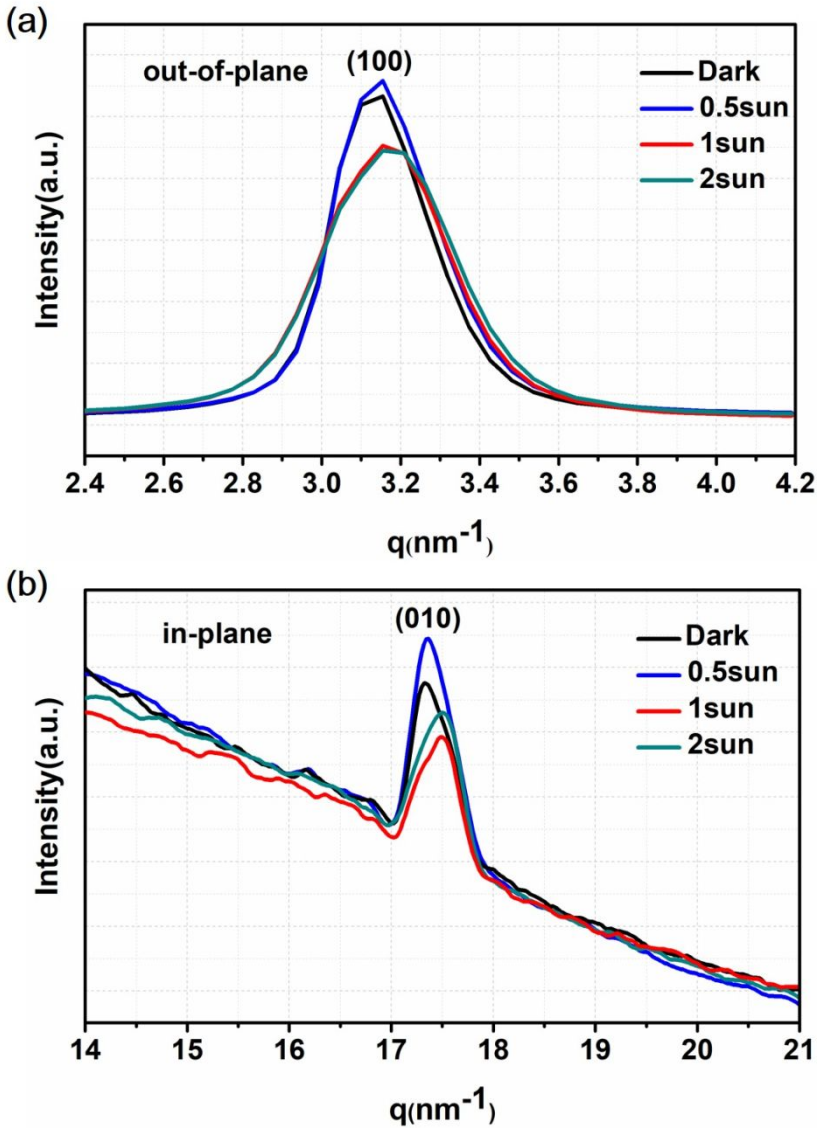

Fig. 2 (a) out-of-plane and (b) in-plane X-ray profiles extracted from GIWAXS for all the samples.

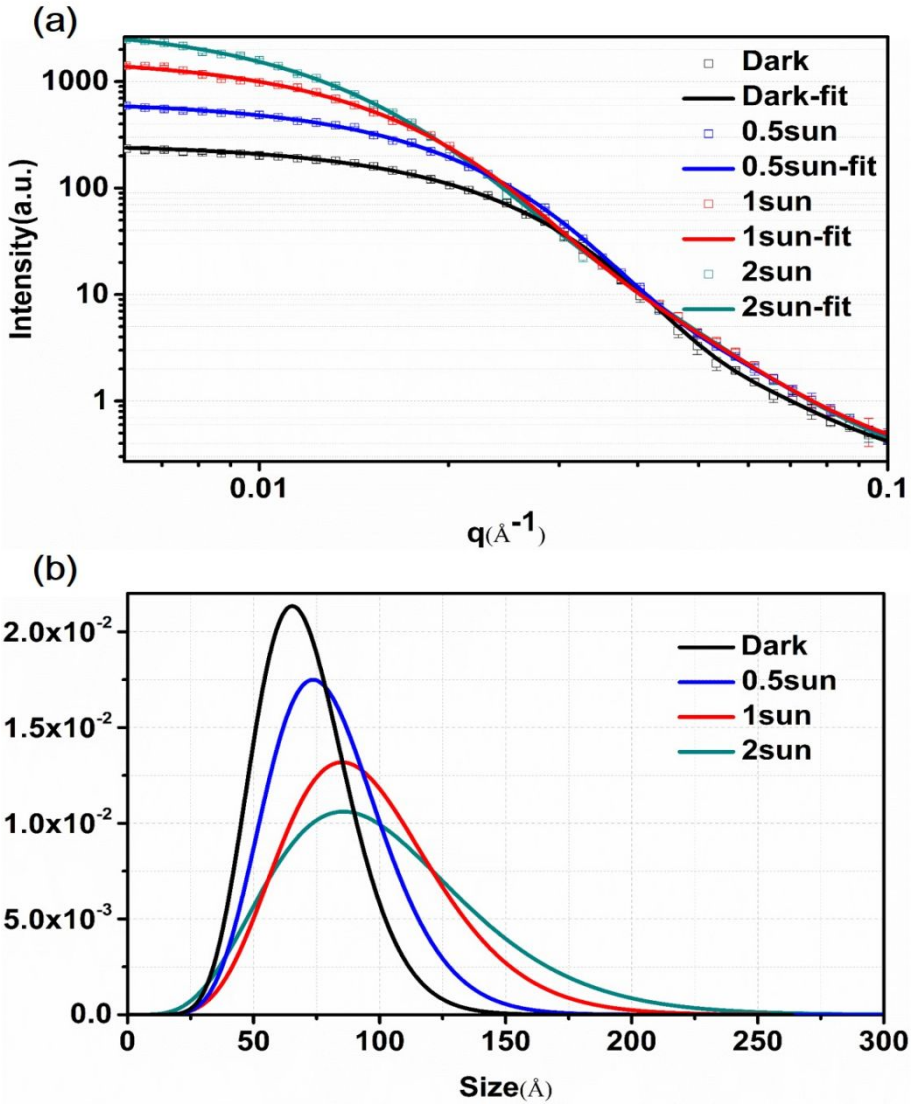

Fig. 3 (a) The absolute small angle neutron scattering intensity with Schulz sphere fitting for p-DTS(FBTTH$_2$)$_2$:PCBM blends and (b) Size distribution of pure PCBM domains in p-DTS(FBTTH$_2$)$_2$:PCBM blends.

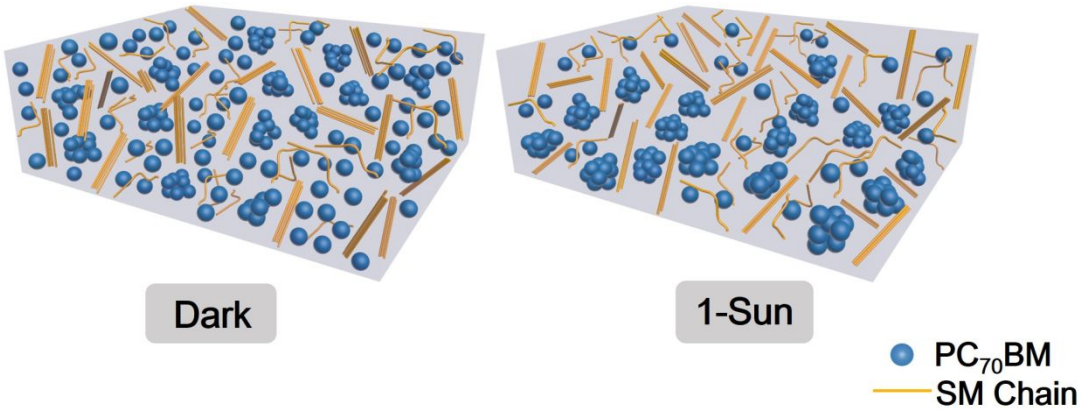

Fig. 4 Schematic drawing of the nanomorphology in p-DTS(FBTTH2)2:PCBM obtained from dark and 1-sun illumination.

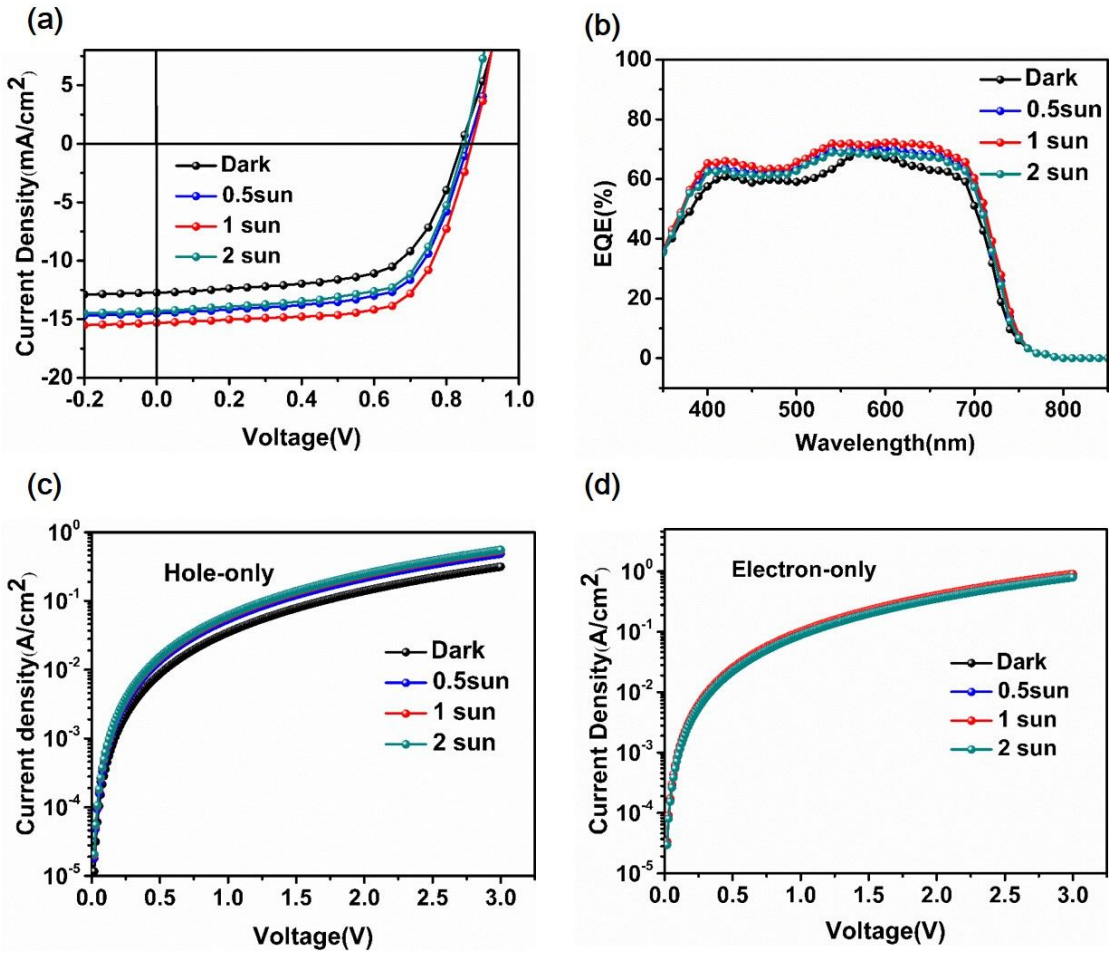

Fig. 5 (a) J-V curves and (b) Normalized external quantum efficiency (EQE) spectra for p-DTS($FBTTH_2$)$_2$:PCBM blends obtained from different light intensities; J-V characteristics for (c) hole-only devices, (d) electron-only devices.

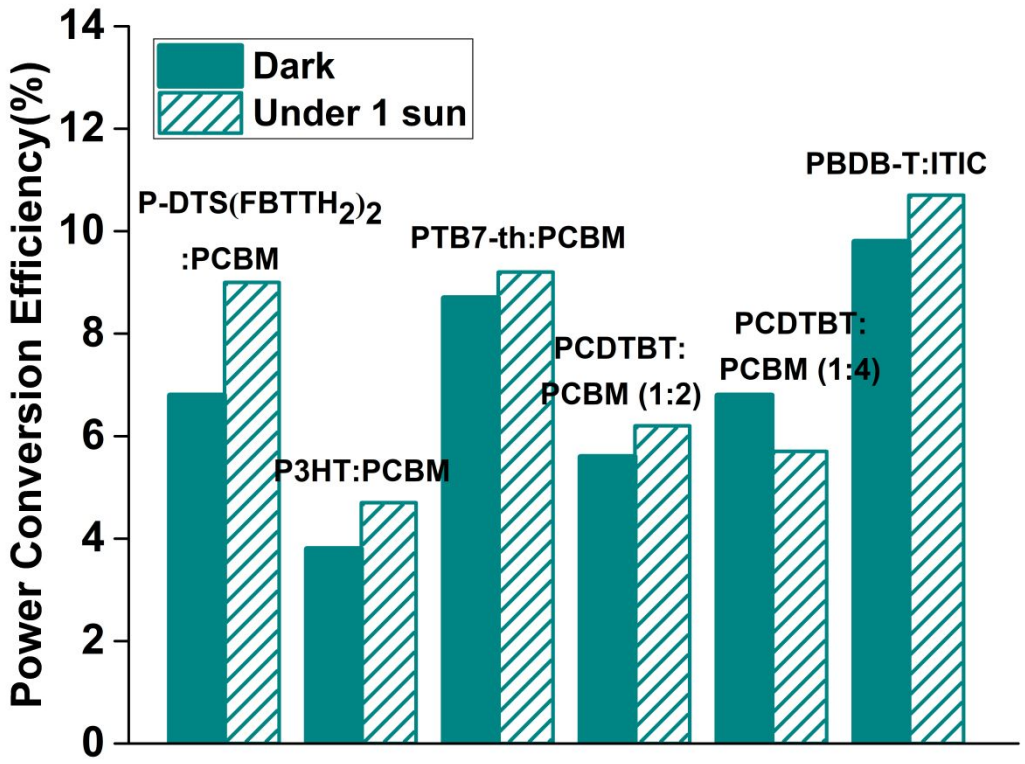

Fig. 6 PCE histogram for different blends under dark and illumination of 1 sun.

Table 1 Coherence length of p-DTS(FBTTH$_2$)$_2$ (ξ),Average radius of pure PCBM domains (R_a), volume fraction of pure PCBM phases (Φ_{ag}), polydispersity of the size of pure PCBM domains (P), and specific interfacial area (S/V) obtained from Schulz sphere model.

	ξ (nm)	Ra(Å)	Φag	P (sig/avg)	S/V (cm^{-1})
Dark	23.4	71	13.2%	0.27	487872
0.5 Sun	20.99	79	17.1%	0.29	534565
1 Sun	17.3	92	20.9%	0.32	573945
2 Sun	15.8	100	23.3%	0.40	527040

Table 2 Area ratios of S(2p) peak /C(1s) peak and N(1s) peak/C(1s) peak for the top surface.

	Dark	0.5 Sun	1 Sun	2 Sun
S(2p) /C(1s)	0.101	0.113	0.122	0.128
N(1s)/C(1s)	0.034	0.038	0.042	0.044

Table 3 Device performance at standard AM-1.5 illumination.

	J_{SC} (mA/cm^2)	V_{OC} (V)	FF (%)	PCE (%)
Dark	12.7±0.2	0.84± 0.03	63.8± 0.4	6.8± 0.2
0.2 Sun	13.3±0.2	0.84±0.02	65.1±0.3	7.27±0.3
0.5 Sun	14.5±0.3	0.86± 0.02	66.1± 0.5	8.2± 0.2
1 Sun	15.3± 0.4	0.87± 0.03	67.7± 0.4	9.0± 0.3
2 Sun	14.3± 0.4	0.85± 0.04	65.7± 0.4	8.0± 0.3

Table 4 Hole and electron mobility calculated from SCLC method.

	Dark	0.5 Sun	1 Sun	2 Sun
Hole mobility ($cm^2V^{-1}s^{-1}$)	2.02×10^{-4}	3.12×10^{-4}	3.46×10^{-4}	3.57×10^{-4}
Electron mobility ($cm^2V^{-1}s^{-1}$)	5.65×10^{-4}	5.72×10^{-4}	5.83×10^{-4}	5.12×10^{-4}

Table of Content

The Effect of Light Environment during Film Formation Process on the Morphology and Function of Organic Photovoltaics

Xiaomin Wu, Shuqiong Lan, Guocheng Zhang, Huipeng Chen* and Tailiang Guo

Light environment during blade coating process has been studied with a result of that crystal sizes of donor material decreased and the size of pure acceptor phase increased with an increase of light intensity along with enhanced phase separation, which shows light environment during blade coating process has a significant impact on morphology, thermodynamics, and device performance of bulk-heterojunction blends.